Integrative Biology

PAPER

Cite this: *Integr. Biol.*, 2018, **10**, 527

Adaptive reorientation of endothelial collectives in response to strain†

Laura Bernardi,‡[a] Costanza Giampietro, ‡[b] Vita Marina,[a] Martina Genta,[a] Edoardo Mazza*[ac] and Aldo Ferrari *[abc]

Received 18th May 2018,
Accepted 3rd August 2018

DOI: 10.1039/c8ib00092a

rsc.li/integrative-biology

Mature epithelial monolayers share the ability to coherently respond to external mechanical stimuli. Tissue remodeling requires cell shape changes and coordinated movements. Human endothelia provide an exquisite example of such emerging collective activities. As part of their function in maintaining body homeostasis under variable hemodynamic loadings, endothelial ensembles must dynamically adapt to wall shear stress and cyclic deformation. While the alignment of several types of cells, including fibroblasts, osteoblasts and epithelial tissues, in response to various flow conditions or wall shear stress levels has been described in detail, less is known about collective endothelial remodeling under pure wall deformation. Here, using a custom-developed bioreactor, we exposed mature human endothelia to two distinct physiological levels of cyclic loading, generating overlapping gradients of strain. Endothelial cells remodeled depending on the level of imposed strain yielding local variations of cell density. In particular, a collective cell orientation orthogonal to the main direction of strain was observed at low levels of wall deformation, while cells reoriented parallel to the main direction of strain at high levels of wall deformation. The tissue adaptation depended on the establishment of mature adherens junctions, which were reinforced by the polarized recruitment of the adaptor protein vinculin. The pivotal role of cell-to-cell junctions was confirmed by the biochemical inhibition of vascular endothelial cadherin homotypic contacts, which impaired the collective remodeling. Together, our data establish wall deformation as an independent determinant of endothelial architecture with direct implications in vascular physiopathology.

Insight, innovation, integration

Hemodynamic loads affect endothelial functions through not completely elucidated mechanisms. Wall shear stress and cyclic wall deformation contribute overlapping mechanical stimuli to which individual cells in a connected monolayer respond collectively. Shape change and migration are coordinated to preserve the tissue integrity. This complex response subtends to an adaptive tissue remodeling having important implications in vascular development and disease. The use of a custom developed bioreactor allows quantifying the response of mature human endothelial to well-defined gradients of strain. The emerging variations of cell density, proliferation, shape and orientation define the tissue adaption to the imposed load. Biochemical interference in this process reveals the central role of vascular-endothelial cadherin in the coordination of tissue remodeling aimed at the polarized reinforcement of cell-to-cell junctions.

Introduction

Human endothelial cells (ECs) form endothelia, connected tissue monolayers that line blood vessels. These unique interfaces regulate mass transfer and maintain body homeostasis.[1] Endothelial architecture requires cells to completely cover the available surface and establish cell-to-substrate adhesions and cell-to-cell junctions with their neighbors.[2] These biological and mechanical cell connections enable collective activities that support multicellular responses and allow functional tissue adaptation to the local environment.[3,4]

The role of molecular signals from circulating moieties has been thoroughly investigated in relation to both endothelial health and disease.[5,6] Less explored is the biomechanical effect of the hemodynamic stresses generated by blood flow. Several works have clearly shown how ECs preferentially orient along

[a] *ETH Zurich, Institute for Mechanical Systems, 8092 Zürich, Switzerland. E-mail: aferrari@ethz.ch, emazza@ethz.ch*
[b] *ETH Zurich, Laboratory for Thermodynamics in Emerging Technologies, 8092 Zürich, Switzerland*
[c] *Empa, Swiss Federal Laboratories for Materials Science and Technology, Überlandstrasse 129, 8600 Dübendorf, Switzerland*

† Electronic supplementary information (ESI) available. See DOI: 10.1039/c8ib00092a

‡ These authors contributed equally to the work.

the direction of flow, in a collective response that can be reproduced *in vitro* using flow bioreactors.[7,8] Cells in the monolayer acquire a coherent polarity yielding cell-to-cell junctions that elongate along the direction of flow.[9] Importantly, when this directional signal is compromised, as in regions of flow recirculation or stenosis, EC orientation and polarization are impaired.[10–13] Besides directionality, flow-generated wall shear stress (WSS) controls the dynamic stability of cell-to-cell junctions acting on vascular endothelial cadherin (VEC[3]). Specifically, VEC-mediated junctions (the adherens junctions, AJs) contribute a range of signals that shape endothelial heterogeneity, yielding characteristic fingerprints of venous and arterial tissues through the recruitment of adaptor proteins, such as vinculin, mediating the interaction with the actin cytoskeleton.[2,4,14,15] This response is intrinsically dynamic, as upon variation of hemodynamic loads the healthy tissue is able to adapt, like during development, workout, or pregnancy.[16–19] On the contrary, maladaptive responses to pathological signals, like those supported by hypertension, lead to endothelial dysfunction and substrate denudation.[20,21]

Cyclic deformation of vessel walls contributes an overlapping mechanical signal (*i.e.* the wall deformation, WD) that acquires particular relevance in arteries.[22,23] Here, loss of wall elasticity accompanies endothelial dysfunction and precedes tissue denudation and atherosclerosis.[24,25] Despite the clear importance, the role of local strain in determining the functional adaptation of ECs and the reorientation of cell-to-cell junctions remains elusive. Some information exists on the individual response of isolated ECs to increasing levels of strain.[26] In the absence of mature junctions, cells reorient along the direction of minimal substrate deformation.[26,27] Specifically, alignment at 70° and 90° is characteristic upon elongation with and without lateral contraction, respectively.[28] In addition, actin stress fibers arrange in parallel bundles oriented perpendicularly to the maximum strain direction.[29] Equi-biaxial strain yields instead a random orientation of isolated ECs.[28] In all these conditions, the degree of reorientation is largely dependent on the deformation magnitude.[26] The deformation rate proves instead less relevant.[28,30] The collective rearrangement of connected monolayers has not been explored to the same extent and single cell analysis is not representative of the *in vivo* situation. The responses of human endothelia to WSS and WD must therefore be decoupled *in vitro* using custom-developed devices capable of applying controlled loads in the physiological and supra-physiological range, for prolonged periods of times, and with full control of the resulting loading maps.[31]

To assess the individual role of mechanical strain on vascular cell structure and function, in the work here presented, monolayers of ECs have been exposed to different levels of cyclic WD, and their response in terms of change in alignment, density and morphology has been analyzed. The *in vivo* deformation of human arteries of healthy adults is variable among the body: strains of about 1–2% have been reported in carotid arteries, 15–20% in human aorta and 2–15% in human femoral arteries.[23,32–34] Based on the range of these values, using a custom-developed bioreactor, we applied to endothelial monolayers two different levels of wall deformation: low (~5% apex strain) and high (~13% apex strain). The here-reported study indicates that ECs in a connected monolayer behave as a multicellular unit and respond to mechanical deformations through the coordinated rearrangement of their cell body orientation. This collective behavior depends on the level and type of imposed mechanical loading and is enabled by functional cell-to-cell junctions.

Results and discussion

Experimental settings

Endothelial monolayers were generated seeding endothelial cells (ECs) at high density on a deformable PDMS membrane (E modulus ~ 1 MPa) previously coated with cross-linked gelatin.[35] After three days in static culture, cells generated a continuous layer featuring homogenous density and well-formed cell-to-cell junctions, as revealed by nuclear and vascular endothelial cadherin (VEC) staining (Fig. 1A, left panel). Specifically, a connectivity index measurement[8] was used to assess the level of AJs maturity (Fig. 1A, right panel). At this stage, ECs in the monolayer did not show any preferential orientation and displayed a circular shape (Table 1), thus indicating fully isotropic culturing conditions.

The PDMS membranes supporting mature monolayers were placed in the bioreactor and exposed to two different loading conditions. The two levels of mechanical loading were selected to reproduce values reported in human arteries or at the luminal surface of pulsatile blood pumping devices, respectively.[36] Specifically, the inflation cylinder was actuated at a physiological frequency of 2 Hz to reach a maximal pressure of 90 or 540 mbar, leading to an equibiaxial strain at the apex of approximately 5% or 13%, in the fully inflated state. The cells were subjected to cyclic loading for a total of 18 h. This time is sufficient for the full adaptation of endothelial monolayers to hemodynamic loadings.[37]

The cyclic membrane actuation generated radial and circumferential gradients of strains on the cell monolayer. Fig. S2A (ESI†) displays a strain–radius plot obtained from the finite element model described in ref. 31. Circumferential and radial strains are reported for both conditions. Specifically, the two strains are equal at the membrane center (up to a distance of ~0.5 mm). Further away from the center they both decrease (Fig. S2A and B, ESI†). However, while the circumferential strain decreases in a monotonic way until the boundary where it tapers to zero, the radial one turns to zero at a radius of ~2 mm from the membrane center. It becomes negative in more peripheral regions, indicating that at the boundary the radial strain is of compression. In summary, the circumferential strain is everywhere greater or equal to the radial one. In the following, the two different loading conditions will be referred to as 5% and 13% (Fig. S2B, ESI†), although the described cellular response involves regions far from the center, which are exposed to strain amplitudes different from the one at the apex.

Collective adaptation of endothelial monolayers

Endpoint analysis of cell density and orientation was performed after 18 h of loading. Five radial regions of interests

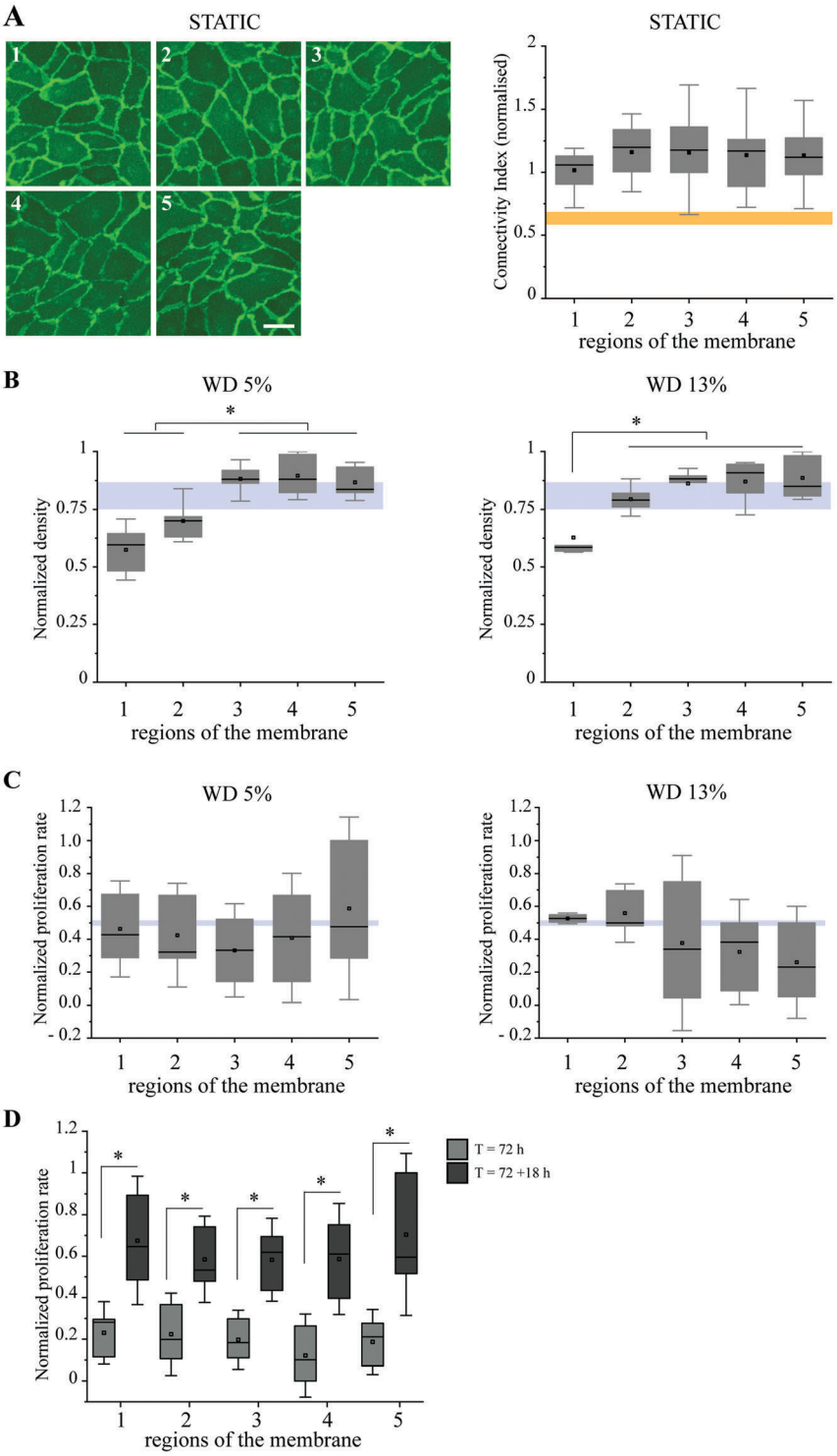

Fig. 1 (A) Representative immunofluorescence analysis of VEC staining (green) in HUVECs cultured in static conditions on different regions of the membrane (left panel) and corresponding quantification of the connectivity index (right panel), $n = 3$ independent experiments. Connectivity index values close to 1 indicate a monolayer with preserved cell-to-cell junctions while values close to zero indicate a diffuse VEC signal in the cytoplasm, typical of ECs with disassembled or immature cell-to-cell junctions. A functional threshold defining differentiated endothelia is measured in recently confluent endothelial monolayer as is identified by as horizontal orange bar. Scale bar: 50 μm. (B) Analysis of cell density in the different regions of the membranes exposed to 5% (left) and 13% (right) strain, $n = 5$ independent experiments, $p < 0.05$. The horizontal bar represent the control values. (C) Quantification of EdU-positive ECs for the proliferation assay in the different regions of the membranes exposed to 5% (left) and 13% (right) strain, $n = 3$ independent experiments. The horizontal bar represents the control values. (D) Quantification of EdU-positive ECs for the proliferation assay in the different regions of the membranes in static condition at the beginning ($T = 72$ h) and at the end ($T = 72 + 18$ h) of the experiments. $n = 3$ independent experiments, $p < 0.05$.

Table 1 Shape index values, the data are means ± standard deviation; n = 5 independent experiments

	5% apex strain (90 mbar)	13% apex strain (540 mbar)	Control
Region 1	0.61 ± 0.15	0.58 ± 0.14	0.75 ± 0.11
Region 2	0.62 ± 0.15	0.60 ± 0.15	0.75 ± 0.11
Region 3	0.60 ± 0.15	0.61 ± 0.14	0.76 ± 0.09
Region 4	0.63 ± 0.16	0.61 ± 0.14	0.75 ± 0.10
Region 5	0.60 ± 0.16	0.64 ± 0.15	0.75 ± 0.10

(ROIs) were defined on the circular membrane (Fig. S2C, ESI†) encompassing areas exposed to different strain cycles.[31] The cell density was measured counting the number of nuclei in each ROI (see Materials and methods). In all tested conditions the lowest value was measured close to the membrane boundary (ctrl: 615 ± 250, 5% strain: 318 ± 150, 13% strain: 362 ± 103 cells per mm^2; ROI 1), and increased moving inward, reaching a maximum in the central ROI where the cell density was equivalent to the one measured on control samples (ctrl: 509 ± 200, 5% strain: 474 ± 187, 13% strain: 520 ± 166 cells per mm^2; ROI 5. Fig. 1B). Specifically, for samples actuated with 5% apex strain (90 mbar), a significant difference in cell density was recorded between ROIs 1–2 and 3–4–5, whereas for the monolayers actuated with 13% apex strain (540 mbar) ROI 1 was statistically different from all others. This data indicates that the applied mechanical loadings impinge in the internal arrangement of endothelial monolayers.

Mechanical strain, detected by mechanoreceptors on the cell surface, induces the activation of intracellular signaling pathways affecting, among other functions, the rate of proliferation, apoptosis, cell structure and morphology.[38] Based on these considerations, the specific effect of mechanical loadings was next analyzed. 18 h of cyclic loading did not affect the rate of proliferation as verified by the DNA incorporation of 5-ethynyl-2′-deoxyuridine (EdU), which directly measures S-phase synthesis of the cell cycle (Fig. 1C). Indeed, no significant differences were detected among different ROIs on membrane actuated at 5% or at 13% apex strain as compared to the static control (Fig. 1C). Same results were obtained measuring the cell proliferation rate at the beginning (t = 0 h) and at the end of the experiments (t = 18 h; Fig. 1D). Comparable proliferation was measured in all ROIs. These results significantly differ from what previously reported in endothelial monolayers exposed to static loads.[39] A static strain of 10%, which reflects the physiological stretch in microvessels, induces cell-cycle re-entry and promotes angiogenic activation and capillary-like endothelial sprouting in confluent and growth arrested endothelial monolayers.[39] Cyclic loading, which represents the physiological stretch in larger vessels, does not affect proliferation (Fig. 1C). Therefore, centripetal migration may contribute to the measured local variations of cell density.

In addition, area measurements were obtained from the distribution of cell-to-cell junction and revealed that cells in ROIs 1 and 2 (close to the boundary) were significantly bigger than cells in ROIs 3–4–5 (towards the center) for both actuating pressures applied (Fig. 2A). The spatial variations in cell surface well correlate with the corresponding values of cell density (Fig. 1B). There is evidence in literature that equi-biaxial strain induces cell shrinkage and reduction of surface area. These data therefore corroborate the finding of increased density under similar loading. These results indicate an inverse correlation between the local cell confluency and the compressive forces generated by neighboring cells, which can restrict movements in jammed monolayers.[40]

Cell morphology is an important descriptor of multicellular activities in monolayers.[41] Elongated cell shapes correlate to unjamming transitions leading to collective cell movements.[42] The shape index (SI, perimeter over surface) of cells,[43] was therefore measured. Values of SI in endothelial monolayers describe the cellular response to shear stress.[43] In all ROIs cells were significantly more elongated as compared to the control (Table 1 and Fig. 2B). In additions, cyclic deformation yielded some variation in the cell shape depending on the distance from the center. Specifically, monolayers actuated with 90 mbar displayed more elongated cells in ROI 1 than in ROI 4 and 5 (Fig. 2B). Corresponding monolayers actuated with 540 mbar featured cells significantly more elongated in ROI 1 and 2 (Table 1) than in the other ROIs (3 to 5). Overall, these results show that ECs subjected to mechanical deformations actively change their morphology. An increased elongation may imply a

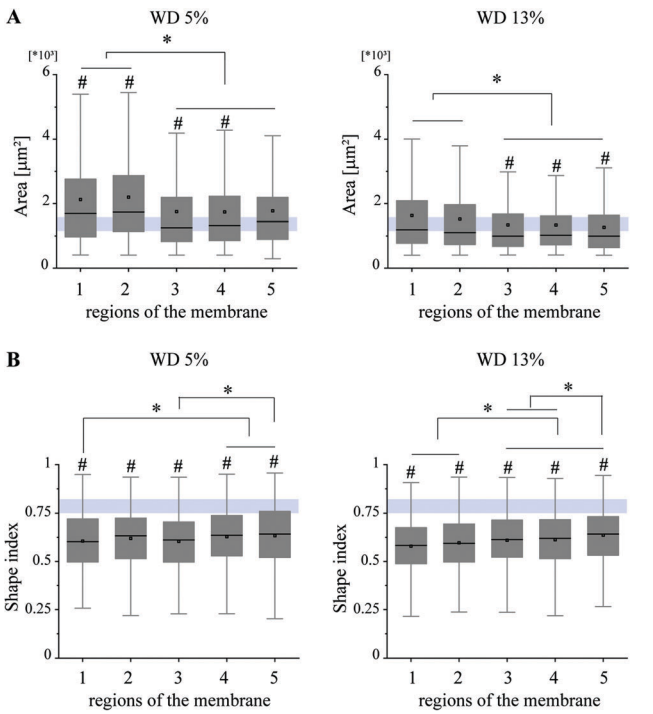

Fig. 2 (A) Analysis of the cell area (μm^2) in the different regions of the membrane exposed to 5% (left) and 13% (right) strain, n = 5 independent experiments, $p < 0.05$. *: statistical significance among the regions of the same test, #: statistical significance between the control and the tested sample for the same region. The horizontal bar represents the control values. (B) Analysis of the shape index (perimeter over surface) in the different regions of the membrane exposed to 5% (left) and 13% (right) strain, n = 5 independent experiments, $p < 0.05$. *: statistical significance among the regions of the same test, #: statistical significance between the control and the tested sample for the same region. The horizontal bar represents the control values.

collective transition in the monolayer, requiring active migration and topological rearrangements.[40]

ECs are elongated in the direction of blood flow in human blood vessels, in response to the local hemodynamic loads.[9] The effect of cyclic deformation on collective cell reorientation was therefore measured in our experimental settings to decouple the cell response to pure strain. As shown in Fig. 3 monolayers actuated with 5% and 13% of WD (90 and 540 mbar pressure, respectively) share common features at the boundary and in the center. At the membrane boundary, cells aligned circumferentially in both conditions of strain, meaning perpendicular to the compressive radial strain, which is in magnitude higher than the circumferential one (zero at the boundary). At the membrane center, cells randomly oriented and were less elongated, as expected since here the circumferential and radial strains are equal. Interestingly, the transition zone (ROIs 3–4) displayed characteristic differences between the two loading conditions. Upon actuation with 5% strain (90 mbar), cells aligned radially, thus perpendicular to the main direction of strain. With 13% strain (540 mbar) cells in the same ROI aligned instead circumferentially, thus parallel to the direction of larger strain. These distributions are rendered by colors in Fig. 4A where rectangular sections of the membranes are reported. Due to the radial symmetry of the sample, these slices are representative of the entire monolayers. In the color-coded maps of cell orientation, warm colors indicate radial orientation, while cold colors the circumferential one. The rose plots in Fig. 4B represent a quantitative description of the same data.

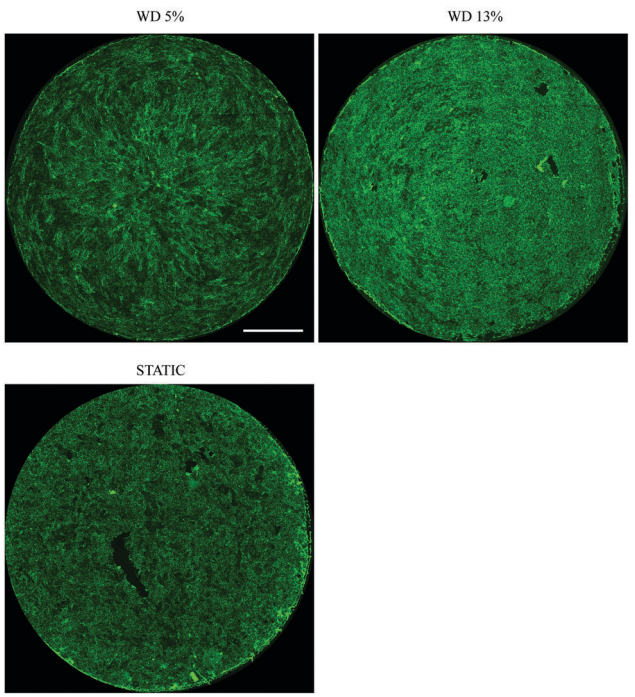

Fig. 3 Representative immunofluorescence of whole membranes exposed to 5% (top, left) and 13% (top, right) loadings at 2 Hz for 18 h and static control (bottom) stained for VEC (green). Cell orientation is clearly visible and the different collective adaptation in the two loading conditions compared to the random static is evident. Scale bar: 1 mm.

When exposed to low levels of WD (5% apex strain, 90 mbar), cells reoriented orthogonally to the main direction of strain, a response that was also reported for isolated cells.[26,27] Under higher levels of WD (13% apex strain, 540 mbar), endothelial collectives produced a different alignment, parallel to the main orientation of strain. Instead, isolated ECs and subconfluent (*i.e.* disconnected) endothelial monolayers reorient perpendicular to the main direction of strain[28] when exposed to large deformations. In all, these results suggest that, under high level of strain, a unique coordinated response emerges in cell collectives, which may be functional to preserve the monolayer integrity.

Tissue morphogenesis, homeostasis, and regeneration require coordinated cellular rearrangements. Collective cell behaviors depend on the organization of cell-to-cell junctions ensuring cohesion, and enabling the barrier function performed by epithelia and endothelia.[1,2,44] AJs may therefore enable collective cell adaptation under high level of cyclic deformation. To verify this hypothesis, the clustering of VEC, the major endothelial-specific transmembrane adhesion protein at AJs,[45] was blocked using a biochemical approach. A specific antibody directed to human VEC ectodomain (clone BV6[46]) was used to inhibit VEC clustering at AJs in monolayers exposed to high loading (540 mbar). As shown in Fig. 4A, BV6 treatments induced VEC removal from cell-to-cell junctions, thus indicating that the correct formation of AJs was impaired. This treatment completely ablated the collective response leading to circumferential alignment in the transition zone (Fig. 4B, Regions 3 and 4). In the treated sample, a random cell alignment was detected. In all, these results suggest that AJs are central regulators of the collective cell orientation in monolayers exposed to high level of strain since that the correct orientation is reached when VEC is correctly clustered at cell-to-cell contacts.

Cell surface receptors integrate mechanical cues to regulate a wide range of biological processes.[47] Among them, the cadherin complex functions as mechanosensory at cell-to-cell junctions.[48,49] In a connected monolayer the mechanical load is transmitted to neighboring cells. Force imbalance at cell-to-cell contacts induces essential morphogenetic processes such as junction remodeling and orientation. However, how cells respond and adapt to the mechanical properties of neighboring cells and transmit forces remain as open questions. To further evaluate the mechanisms driving cell reorientation under high strain, vinculin localization at AJs was analyzed. Intercellular forces coincide with vinculin accumulation at cadherin adhesions, where the protein potentiates cadherin mechanosensory response.[14] In addition, in endothelial monolayers, junction remodeling occurs only in a subset of VEC adhesions, which experience significant tension, and are therefore revealed by the accumulation of the mechanosensory protein vinculin.

Fig. 5 reports the immunofluorescence (Fig. 5A) and relative quantification (Fig. 5B) of vinculin distribution at VEC junction sites. Co-localization was more pronounced at the cell-to-cell junctions of monolayers exposed for 18 h to low level of deformation (radially oriented), than in monolayers exposed to the high level of deformation (circumferentially oriented). This result supports the hypothesis that, in case of larger deformations,

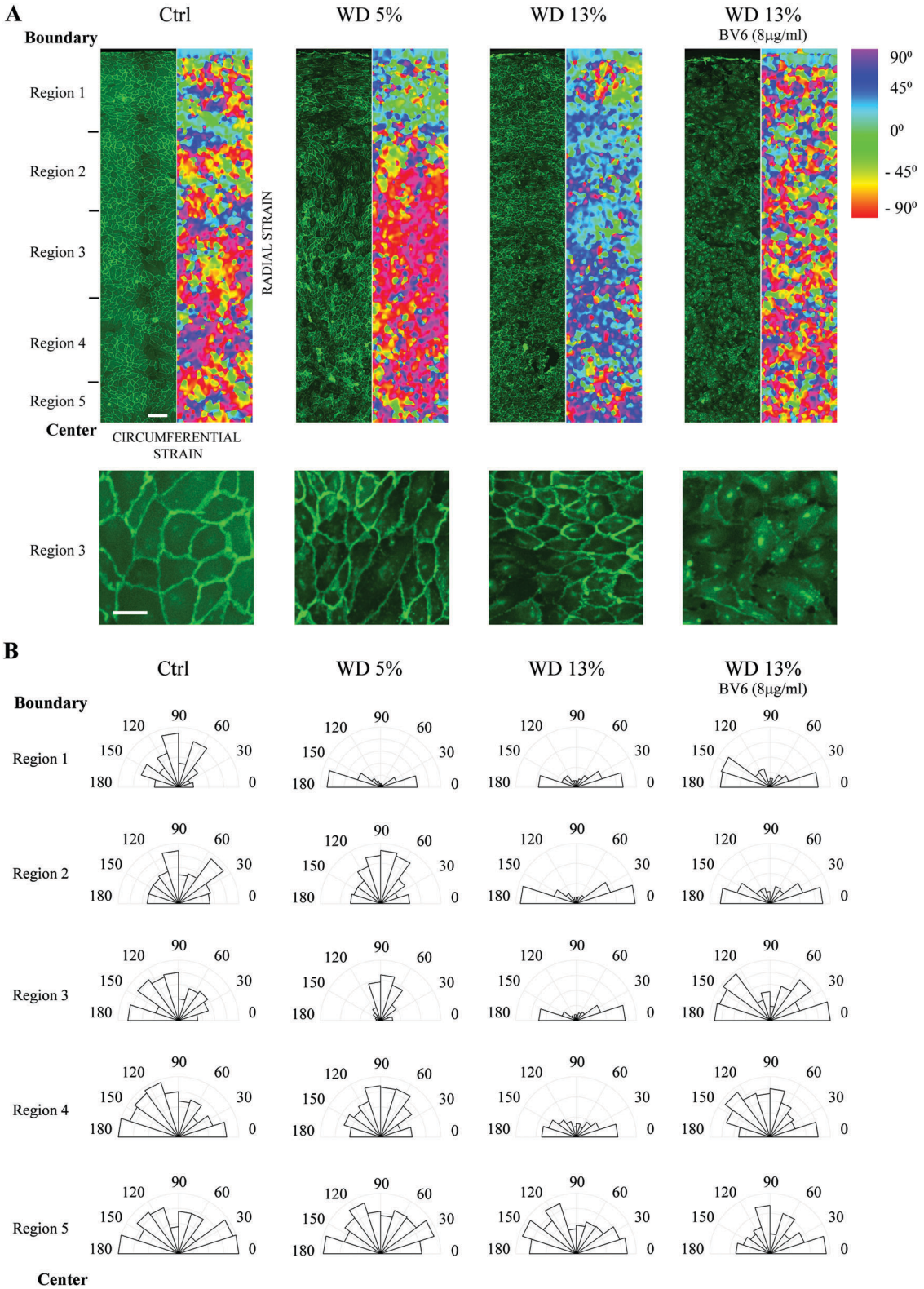

Fig. 4 (A) Representative sections of the membranes stained with VEC (green, left) and color plots of the cell orientation (right). Scale bar: 100 μm. Bottom panels: magnifications of part of Region 3, scale bar: 20 μm. (B) Rose plot of the orientation angles. The orientation has been analyzed in the 5 regions of the membrane; n = 5 independent experiments for 5% and 13% strain, n = 3 independent experiments for control and 13% strain +BV6 treatment.

ECs reorient parallel to the main direction of strain to minimize the tension at the AJs thus contributing to maintain monolayer integrity. When endothelial monolayers were exposed to high strain for a shorter period of time (1 h) an intermediate reorientation state

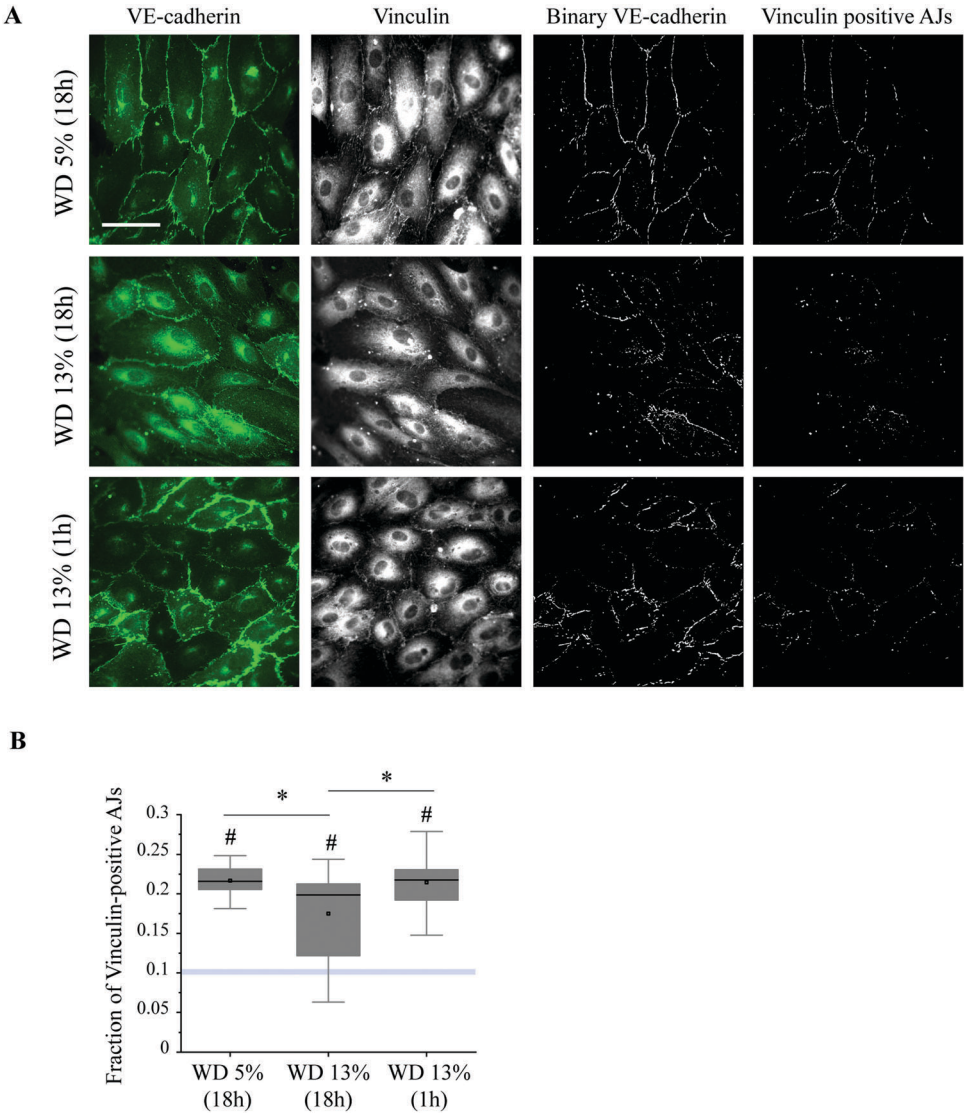

Fig. 5 (A) Representative immunofluorescence analysis of VEC (green) and vinculin (gray scale) on membranes (Region 3) exposed to 5% and 13% strain for 18 h and to 13% strain for 1 h. The corresponding binarized images of VEC and the vinculin-positive AJs are reported. (B) Quantification of the fraction of vinculin-positive AJs; $n = 2$ independent experiments, 16 images for each condition have been analyzed. *: statistical significance among the regions of the same test, #: statistical significance between the control and the tested sample for the same region. The horizontal bar represents the control values.

was captured. Here cells in the monolayer started to reorient along the circumferential direction. The fraction of vinculin-positive AJs was higher to that measured at 18 h. This subset of junctions undergoing remodeling was higher at the beginning of the loading, but was reduced upon complete cell reorientation, further corroborating the hypothesis that under high cyclic strain ECs adapt their orientation to minimize the tension at the junctions.

Conclusion

This work studies the behavior of mature and connected endothelial monolayers exposed to different levels of cyclic deformation using a custom-developed bioreactor. Two main novel observations are reported. First, the mechanical loading affects the overall cell density in the monolayer. This is mainly achieved thought the remodeling of endothelial cell morphology. Second, endothelial collectives adaptively respond to mechanical deformations and reorient depending on the level of imposed strain. The correct establishment of AJs drives this coordinated response. VEC is the mechanosensory receptor triggering this adaptation, which proceeds through the recruitment of vinculin at the junctional complex.

Few studies have investigated the response of endothelial collectives to cyclic deformation.[50–52] More information exists on the cellular response to wall shear stress.[3,7,8,15,37,53,54] Despite the differences in the specific experimental settings, it is worth noting that cells in monolayers exposed to high shear reorient perpendicular to the flow, whereas a parallel alignment is typical under low wall shear stress loadings.[8] Interestingly, for

both shear stress and deformation, connected endothelial ensembles show two alternative states of collective reorientation, which are preferentially adopted depending on the loading values. When a threshold of the stimulus is overtaken, the cells reorient in the opposite direction. While the mechanisms behind this behavior are still elusive, the multicellular response to both the mechanical loadings may share common features.

Strain-induced cell reorientation is a broad phenomenon, which goes beyond the reported effect on endothelial tissues. Cyclic substrate stretching is physiologically sustained by breathing, heart beating and blood vessel pulsation. When subjected to periodic loading, several type of cells, including fibroblasts and osteoclasts, align nearly perpendicular to the primary stretch direction. In particular, the extent of cell reorientation correlates with the stretch magnitude.[28,55–60] A striking example of collective reorientation is represented by developing epithelial tissues. Epithelial morphogenesis depends on internally-generated forces which collectively affect tissue architecture.[61] Individual cells in the monolayer exert forces on their neighbors and on the substrate, through specialized junctional complexes.[42] The overall force balance defines the transition to collective jamming which appears upon cell density increase[62] and can be reverted upon wound healing or pathological insults.[40] Previous reports provide much information on how epithelial tissues remodel when exposed to substrate stretching for long periods. Uniaxial stretch induces a collective reorientation of cells in the monolayer along the direction of deformation.[63] Other physiologically-relevant loading conditions, such as biaxial cyclic stretches[64] induced instead tissue rupture and cell death proportional to the level of stretch applied.[64,65] These differences between epithelial and endothelial collective behavior highlight a remarkable higher degree of plasticity of endothelium.

Although further studies are needed to fully clarify the precise nature of the biochemical and mechanical mechanisms and processes leading to the described coordinated response, the results here reported provide means for investigating cell behavior under a range of specific hemodynamic condition. Moreover, they make clear that cyclic deformation is an important determinant of vascular wall biology, possibly controlling the correct homeostasis and standing at the origins of maladaptive endothelial responses such as those leading to atherosclerosis or implicated in the development of aneurism.

Materials and methods

Sample preparation

PDMS membranes of 390 ± 10 μm thickness were fabricated as previously reported.[31,66] Before usage, membranes were treated with plasma (100 W for 30 s, 1 ± 0.2 mbar)[31] to increase hydrophilicity and then coated with 1.5% gelatin (104070, Merck Millipore, USA) to promote cell adhesion as previously described.[37]

Cell culture and treatments

Primary Human Umbilical Vein Endothelial Cells (HUVECs; Invitrogen, USA) were grown in medium 200PRF supplemented with fetal bovine serum 2% v/v, hydrocortisone 1 mg ml^{-1}, human epidermal factor 10 ng ml^{-1}, basic fibroblast growth factor 3 ng ml^{-1} and heparin 10 mg ml^{-1} (all reagents from Invitrogen, USA) and were maintained at 37 °C and 5% CO_2. Experiments were performed using cells from 2 to 6 passages *in vitro*. To obtain a confluent monolayer, 5×10^4 cells per cm^2 were seeded on membranes and cultured for three days.[37] To investigate the role of AJs in the orientation of the cells, endothelial monolayers were pre-incubated for 30 min with a blocking antibody against VE-cadherin (anti-VE-cadherin, clone BV6, EMD Millipore Corporation, Temecula, CA, USA[46]) at a concentration of 8 μg ml^{-1}.

Finite element model

A finite element model of the inflation system was created using ABAQUS (Abaqus 6.9-1, Dassault Systèmes). The model was 2D axial symmetric (*x*–*y* plane, *x* being the radial axis and *y* being the vertical axis). 8-Node biquadratic axisymmetric quadrilateral, hybrid, linear pressure, reduced integration elements were selected for all computations. The constitutive model applied for the PDMS membrane was the one determined in our previous investigations on the multiaxial large strain mechanical behavior of the material.[67] The membrane edge was constrained in the vertical and radial direction, to simulate the boundary conditions applied in the real system. The pressure loading was applied on the bottom surface of the membrane.

Proliferation assay

The DNA synthesis – based cell proliferation assay was performed using a commercially-available Click-iT EdU Imaging Kits Protocol (Thermo Fisher Scientific) and following the manufacturer recommendations. After three days in culture, endothelial monolayers were incubated for 1 h with 10 μM 5-ethynyl-2′-deoxyuridine (EdU) labeling solution and then, some samples were fixed and others, after replacement with full media, were incubated for 18 h in static conditions or subjected to 18 h of mechanical loading experiments. At the end of the experiments, cells were fixed with 4% formaldehyde, permeabilized with 0.5% Triton X-100 in PBS, processed and immediately imaged using a fluorescence microscope.

Mechanical loading experiments

A custom-developed dynamic bioreactor[31] was exploited to decouple the effect of pulsatile wall deformation (WD) on endothelial monolayers. Briefly, the bioreactor comprises two components: a medium chamber and an inflation cylinder (Fig. S1A, ESI†). The chamber housing the cells under analysis is filled with warm medium and connected to a medium reservoir by two Tygon tubes of 0.8 cm in diameter. In particular, the reservoir consists of a sterile glass bottle with ventilated cap containing 50 ml of complete medium. The entire system is maintained in an incubated environment (37 °C, 95% humidity, and 5% CO_2) for the full duration of the loading experiments, therefore ensuring full metabolic supply to the cells.

The inflation system actuates cyclic stretch on a deformable membrane covered by ECs. The membrane is comprised of a PDMS-based elastomer, which faces the medium chamber and

supports the endothelial monolayer at its luminal surface. The membrane inflation system is composed of a cylinder of 15 mm outer diameter and 5 mm inner diameter fixed to the flow chamber by 4 screws (Fig. S1B, ESI†). Sealing was obtained with an O-ring interposed between the membrane and the cylinder. The volume of liquid (*i.e.* PBS) inside the cylinder is controlled with a syringe pump (PSD/4 HAMILTON, Bonaduz, equipped with a 5 ml glass syringe) receiving on-line feedback from a pressure sensor (MPX 4250 AP, Freescale). The luminal end of the cylinder extends towards the medium chamber and is separated from it by the interfacing deformable membrane. Therefore, the hydrostatic pressure in the cylinder actuates the cyclic inflation of the membrane during the experiment. During the stretching loop, the deformable PDMS membrane cycles between two states: the flat state (Fig. S1C (ESI†), left panel) during which the substrate is in its reference configuration (*i.e.* no WD), and the inflated state (Fig. S1C (ESI†), right panel) during which the maximal imposed stretch is reached (*i.e.* maximal WD). The whole system is placed inside a cell incubator in a humidified atmosphere of 5% CO_2 at 37 °C for the entire duration of the experiments.

In preparation to the cell experiments, the bioreactor,[31] flow tubes and connecting tubes were cleaned by immersion in 70% ethanol followed by extensive washing in PBS, and the reservoir was autoclaved. The system was mounted under a biological hood in sterile condition. After it was filled with warm medium, membranes covered with endothelial monolayers were sited inside the system.

The bioreactor was then placed into the incubator and all the connectors were fastened. Once the inflation circuit was filled with PBS (for details see ref. 31), the test was started.

Three different conditions of experiments were tested. In the first set, tests were performed at a pressure of 90 mbar and 540 mbar, corresponding to ~5% (low value) and ~13% (high value) apex strain, respectively. The selected values are within the physiological range.[36] The cycle frequency was set to 2 Hz and the total duration of each test was 18 h, according to ref. 31. In the second set, membranes were exposed to 540 mbar pressure at a frequency of 2 Hz for 18 h and cells were incubated with a specific antibody directed to human VEC ectodomain (clone BV6) to inhibit VEC clustering at AJs; while in the third were exposed to 540 mbar at a frequency of 2 Hz for 1 h.

Antibodies

The following primary antibodies were used: goat anti-VE-cadherin (1:200, Santa Cruz Biotechnology Inc., USA; #6458), mouse anti-vinculin (1:400, Sigma Aldrich, USA, #V9131) TRITC-phalloidin (Sigma Aldrich, USA, #P1951). The secondary antibodies (1:400) were donkey anti-goat Alexa 488 (Invitrogen, USA) and chicken anti-mouse-Alexa 647 (Invitrogen, USA) For staining of nuclei, Hoechst was added at 10 mg ml^{-1}.

Immunostaining and imaging

HUVECs were fixed with 3% paraformaldehyde (PFA) for 20 min and permeabilized and 0.1% Triton-X100 in PBS for 10 min at room temperature (RT). After washing the samples three times for 5 min with PBS, they were incubated with 5% bovine serum albumin (BSA) in PBS for 2 h at RT. Samples were incubated with primary antibody overnight at 4 °C. Subsequently, the samples were rinsed four times for 1 h each with 5% BSA in PBS and then incubated with TRITC-phalloidin (Sigma, USA) and secondary antibodies for 45 min at RT. Finally, samples were washed three times in PBS, post-fixed for 2 min in 3% PFA, briefly washed again with PBS, mounted with mounting medium and immediately imaged. Imaging of the whole membrane was obtained by stitching several images acquired with an inverted Nikon-Ti spinning disk confocal microscope (Nikon, Japan) equipped with a 20× air objective, 0.75 NA. High magnification images were obtained using a 60× oil objective, 1.4 NA.

Data analysis

A custom-made code was created for the image analysis of cell density, shape index and orientation.

The image of the membrane was divided in to 9 × 9 squares of ~0.55 μm length each (Fig. S1A, ESI†). The nuclei channel (wavelength 395 nm) was used for the cell density calculation. The Fiji function ''Analyse Particle''[68,69] and a script written in commercial software package (MATLAB 2015b, The MathWorks Inc., Natick, MA, 2000) were used to count the cells inside each square and create density maps. For each membrane, the number of nuclei of each square was normalized by the number of nuclei of the square containing the highest of them. The VE-cadherin channel (wave length 470) was used for cell segmentation *via* manual tracking of the cell boundary of ~50 cells per square of 5 squares (indicated in Fig. S1A, ESI†). Due to the axial symmetry, these squares are representative of the whole membrane. An ellipse was then fitted to each cell, and its major axis was used to extract the cell direction. Orientation color plots were created using the ImageJ plugin ''OrientationJ''.[70–72] Furthermore, cell area, perimeter and shape index were calculated from the fitted ellipse parameters. Shape index is calculated as $SI = 4\pi A/P^2$, being A the cell area and P the cell perimeter, respectively. A SI of 1 indicates a perfect circle, whereas a SI of 0 a straight line.[43]

To calculate the fraction of vinculin positive junctions, a method similar to the one presented in ref. 14 was developed in Fiji. Briefly, VE-cadherin and the vinculin images were background subtracted using the ''Subtract Background'' function of Fiji (''rolling = 5''), then a user defined value was subtracted from the image (''Subtract'' function, ''value = 5''). After the images were converted to 32-bit and then made binary. The two resulting images were multiplied (''Image Calculator, Multiply'' function). The final image contains the overlapping areas, were both VE-cadherin and vinculin signals are present. The number of white pixels (containing the signal) of the overlapping image was divided by the number of the white pixels of the VEC binary image. This ratio gives the fraction of vinculin positive junctions.

To evaluate the monolayer integrity a connectivity index (CI) measurement was performed to reveal the distribution of VEC at the cell membrane.[8] CI values close to 1 are indicative of a monolayer with a fully retained network of cell-to-cell junctions, while values close to 0 report of a diffuse VEC signal

in the cytoplasm, typical of cells with disassembled or immature junctions. A threshold value is set at 0.6, corresponding to the transition between a recently confluent and a mature endothelium.[73]

Statistical analysis

Variations between the tests were identified using a non-parametric Mann–Whitney, $p < 0.05$. Boxes in all box plots span from 1st to 3rd quartile, outliers were removed from the plot. Black lines indicate the medians. Whiskers extend to 1.5× IQR (inter-quantile range). Where present, asterisks indicate a significant difference among regions of the same type of test, while number signs indicate a significant difference between the control and the tested sample for the same region.

Conflicts of interest

The authors declare no competing financial interests.

Acknowledgements

This project was supported by the ''Stiftung PROPTER HOMINES – Vaduz/Fürstentum Liechtenstein'', the ''Schwyzer-Winiker Stiftung'', the ''Mäxi-Stiftung'' and the ETH Zurich Foundation. This work is part of the Zurich Heart project of Hochschulmedizin Zürich under the umbrella of ''University Medicine Zurich/Hochschulmedizin Zurich''.

References

1 E. Dejana and C. Giampietro, Vascular endothelial-cadherin and vascular stability, *Curr. Opin. Hematol.*, 2012, **19**, 218–223.
2 E. Dejana, Endothelial cell-cell junctions: happy together, *Nat. Rev. Mol. Cell Biol.*, 2004, **5**, 261–270.
3 F. Orsenigo, C. Giampietro, A. Ferrari, M. Corada, A. Galaup, S. Sigismund, G. Ristagno, L. Maddaluno, G. Y. Koh, D. Franco, V. Kurtcuoglu, D. Poulikakos, P. Baluk, D. McDonald, M. Grazia Lampugnani and E. Dejana, Phosphorylation of VE-cadherin is modulated by haemodynamic forces and contributes to the regulation of vascular permeability in vivo, *Nat. Commun.*, 2012, **3**, 1208.
4 Y. L. Dorland and S. Huveneers, Cell-cell junctional mechanotransduction in endothelial remodeling, *Cell. Mol. Life Sci.*, 2017, **74**, 279–292.
5 S. M. Camus, J. A. De Moraes, P. Bonnin, P. Abbyad, S. Le Jeune, F. Lionnet, L. Loufrani, L. Grimaud, J. C. Lambry, D. Charue, L. Kiger, J. M. Renard, C. Larroque, H. Le Clesiau, A. Tedgui, P. Bruneval, C. Barja-Fidalgo, A. Alexandrou, P. L. Tharaux, C. M. Boulanger and O. P. Blanc-Brude, Circulating cell membrane microparticles transfer heme to endothelial cells and trigger vasoocclusions in sickle cell disease, *Blood*, 2015, **125**, 3805–3814.
6 T. J. Rabelink, H. C. de Boer and A. J. van Zonneveld, Endothelial activation and circulating markers of endothelial activation in kidney disease, *Nat. Rev. Nephrol.*, 2010, **6**, 404–414.
7 D. Franco, F. Milde, M. Klingauf, F. Orsenigo, E. Dejana, D. Poulikakos, M. Cecchini, P. Koumoutsakos, A. Ferrari and V. Kurtcuoglu, Accelerated endothelial wound healing on microstructured substrates under flow, *Biomaterials*, 2013, **34**, 1488–1497.
8 F. Robotti, D. Franco, L. Banninger, J. Wyler, C. T. Starck, V. Falk, D. Poulikakos and A. Ferrari, The influence of surface micro-structure on endothelialization under supraphysiological wall shear stress, *Biomaterials*, 2014, **35**, 8479–8486.
9 E. Tzima, M. Irani-Tehrani, W. B. Kiosses, E. Dejana, D. A. Schultz, B. Engelhardt, G. Cao, H. DeLisser and M. A. Schwartz, A mechanosensory complex that mediates the endothelial cell response to fluid shear stress, *Nature*, 2005, **437**, 426–431.
10 S. Chien, Effects of disturbed flow on endothelial cells, *Ann. Biomed. Eng.*, 2008, **36**, 554–562.
11 T. Zand, J. J. Nunnari, A. H. Hoffman, B. J. Savilonis, B. MacWilliams, G. Majno and I. Joris, Endothelial adaptations in aortic stenosis. Correlation with flow parameters, *Am. J. Pathol.*, 1988, **133**, 407–418.
12 B. L. Langille and S. L. Adamson, Relationship between blood flow direction and endothelial cell orientation at arterial branch sites in rabbits and mice, *Circ. Res.*, 1981, **48**, 481–488.
13 J. J. Chiu and S. Chien, Effects of disturbed flow on vascular endothelium: pathophysiological basis and clinical perspectives, *Physiol. Rev.*, 2011, **91**, 327–387.
14 S. Huveneers, J. Oldenburg, E. Spanjaard, G. van der Krogt, I. Grigoriev, A. Akhmanova, H. Rehmann and J. de Rooij, Vinculin associates with endothelial VE-cadherin junctions to control force-dependent remodeling, *J. Cell Biol.*, 2012, **196**, 641–652.
15 F. le Noble, D. Moyon, L. Pardanaud, L. Yuan, V. Djonov, R. Matthijsen, C. Breant, V. Fleury and A. Eichmann, Flow regulates arterial-venous differentiation in the chick embryo yolk sac, *Development*, 2004, **131**, 361–375.
16 D. S. Boeldt and I. M. Bird, Vascular adaptation in pregnancy and endothelial dysfunction in preeclampsia, *J. Endocrinol.*, 2017, **232**, R27–R44.
17 L. Slavik, J. Prochazkova, M. Prochazka, O. Simetka, A. Hlusi and J. Ulehlova, The pathophysiology of endothelial function in pregnancy and the usefulness of endothelial markers, *Biomed. Pap. Med. Fac. Univ. Palacky Olomouc Czech Repub.*, 2011, **155**, 333–337.
18 P. M. Haram, V. Adams, O. J. Kemi, A. O. Brubakk, R. Hambrecht, O. Ellingsen and U. Wisloff, Time-course of endothelial adaptation following acute and regular exercise, *Eur. J. Cardiovasc. Prev. Rehabil.*, 2006, **13**, 585–591.
19 P. M. Haram, O. J. Kemi and U. Wisloff, Adaptation of endothelium to exercise training: insights from experimental studies, *Front. Biosci.*, 2008, **13**, 336–346.
20 R. P. Brandes, Endothelial dysfunction and hypertension, *Hypertension*, 2014, **64**, 924–928.
21 D. Konukoglu and H. Uzun, Endothelial Dysfunction and Hypertension, *Adv. Exp. Med. Biol.*, 2017, **956**, 511–540.

22 H. C. Han and Y. C. Fung, Longitudinal strain of canine and porcine aortas, *J. Biomech.*, 1995, **28**, 637–641.

23 G. Choi, L. K. Shin, C. A. Taylor and C. P. Cheng, In vivo deformation of the human abdominal aorta and common iliac arteries with hip and knee flexion: implications for the design of stent-grafts, *J. Endovasc. Ther.*, 2009, **16**, 531–538.

24 A. Tokita, Y. Ishigaki, H. Okimoto, H. Hasegawa, Y. Koiwa, M. Kato, H. Ishihara, Y. Hinokio, H. Katagiri, H. Kanai and Y. Oka, Carotid arterial elasticity is a sensitive atherosclerosis value reflecting visceral fat accumulation in obese subjects, *Atherosclerosis*, 2009, **206**, 168–172.

25 R. Cernes, R. Zimlichman and M. Shargorodsky, Arterial elasticity in cardiovascular disease: focus on hypertension, metabolic syndrome and diabetes, *Adv. Cardiol.*, 2008, **45**, 65–81.

26 R. Kaunas, P. Nguyen, S. Usami and S. Chien, Cooperative effects of Rho and mechanical stretch on stress fiber organization, *Proc. Natl. Acad. Sci. U. S. A.*, 2005, **102**, 15895–15900.

27 M. Moretti, A. Prina-Mello, A. J. Reid, V. Barron and P. J. Prendergast, Endothelial cell alignment on cyclically-stretched silicone surfaces, *J. Mater. Sci.: Mater. Med.*, 2004, **15**, 1159–1164.

28 J. H. Wang, P. Goldschmidt-Clermont, J. Wille and F. C. Yin, Specificity of endothelial cell reorientation in response to cyclic mechanical stretching, *J. Biomech.*, 2001, **34**, 1563–1572.

29 S. Chien, Mechanotransduction and endothelial cell homeostasis: the wisdom of the cell, *Am. J. Physiol. Heart Circ. Physiol.*, 2007, **292**, H1209–H1224.

30 A. M. Greiner, S. A. Biela, H. Chen, J. P. Spatz and R. Kemkemer, Temporal responses of human endothelial and smooth muscle cells exposed to uniaxial cyclic tensile strain, *Exp. Biol. Med.*, 2015, **240**, 1298–1309.

31 B. J. Bachmann, L. Bernardi, C. Loosli, J. Marschewski, M. Perrini, M. Ehrbar, P. Ermanni, D. Poulikakos, A. Ferrari and E. Mazza, A Novel Bioreactor System for the Assessment of Endothelialization on Deformable Surfaces, *Sci. Rep.*, 2016, **6**, 38861.

32 P. B. Dobrin, Mechanical properties of arteries, *Physiol. Rev.*, 1978, **58**, 397–460.

33 T. M. Morrison, G. Choi, C. K. Zarins and C. A. Taylor, Circumferential and longitudinal cyclic strain of the human thoracic aorta: age-related changes, *J. Vasc. Surg.*, 2009, **49**, 1029–1036.

34 A. Wittek, K. Karatolios, C. P. Fritzen, J. Bereiter-Hahn, B. Schieffer, R. Moosdorf, S. Vogt and C. Blase, Cyclic three-dimensional wall motion of the human ascending and abdominal aorta characterized by time-resolved three-dimensional ultrasound speckle tracking, *Biomech. Model. Mechanobiol.*, 2016, **15**, 1375–1388.

35 M. G. Lampugnani, M. Corada, P. Andriopoulou, S. Esser, W. Risau and E. Dejana, Cell confluence regulates tyrosine phosphorylation of adherens junction components in endothelial cells, *J. Cell Sci.*, 1997, **110**(Pt 17), 2065–2077.

36 S. J. Sonntag, T. A. S. Kaufmann, M. R. Busen, M. Laumen, T. Linde, T. Schmitz-Rode and U. Steinseifer, Simulation of a pulsatile total artificial heart: development of a partitioned fluid structure interaction model, *J. Fluids Struct.*, 2013, **38**, 187–204.

37 G. Stefopoulos, C. Giampietro, V. Falk, D. Poulikakos and A. Ferrari, Facile endothelium protection from TNF-alpha inflammatory insult with surface topography, *Biomaterials*, 2017, **138**, 131–141.

38 N. F. Jufri, A. Mohamedali, A. Avolio and M. S. Baker, Mechanical stretch: physiological and pathological implications for human vascular endothelial cells, *Vasc. Cell*, 2015, **7**, 8.

39 A. S. Zeiger, F. D. Liu, J. T. Durham, A. Jagielska, R. Mahmoodian, K. J. Van Vliet and I. M. Herman, Static mechanical strain induces capillary endothelial cell cycle re-entry and sprouting, *Phys. Biol.*, 2016, **13**, 046006.

40 C. Malinverno, S. Corallino, F. Giavazzi, M. Bergert, Q. Li, M. Leoni, A. Disanza, E. Frittoli, A. Oldani, E. Martini, T. Lendenmann, G. Deflorian, G. V. Beznoussenko, D. Poulikakos, O. K. Haur, M. Uroz, X. Trepat, D. Parazzoli, P. Maiuri, W. Yu, A. Ferrari, R. Cerbino and G. Scita, Endocytic reawakening of motility in jammed epithelia, *Nat. Mater.*, 2017, **16**, 587–596.

41 L. Atia, D. Bi, Y. Sharma, J. A. Mitchel, B. Gweon, S. A. Koehler, S. J. DeCamp, B. Lan, J. H. Kim, R. Hirsch, A. F. Pegoraro, K. H. Lee, J. R. Starr, D. A. Weitz, A. C. Martin, J.-A. Park, J. P. Butler and J. J. Fredberg, Geometric constraints during epithelial jamming, *Nat. Phys.*, 2018, **14**, 613–620.

42 J. A. Park, L. Atia, J. A. Mitchel, J. J. Fredberg and J. P. Butler, Collective migration and cell jamming in asthma, cancer and development, *J. Cell Sci.*, 2016, **129**, 3375–3383.

43 M. J. Levesque, D. Liepsch, S. Moravec and R. M. Nerem, Correlation of endothelial cell shape and wall shear stress in a stenosed dog aorta, *Arteriosclerosis*, 1986, **6**, 220–229.

44 P. Friedl and R. Mayor, Tuning Collective Cell Migration by Cell-Cell Junction Regulation, *Cold Spring Harbor Perspect. Biol.*, 2017, **9**, a029199, DOI: 10.1101/cshperspect.a029199.

45 E. Dejana, F. Orsenigo and M. G. Lampugnani, The role of adherens junctions and VE-cadherin in the control of vascular permeability, *J. Cell Sci.*, 2008, **121**, 2115–2122.

46 M. Corada, F. Liao, M. Lindgren, M. G. Lampugnani, F. Breviario, R. Frank, W. A. Muller, D. J. Hicklin, P. Bohlen and E. Dejana, Monoclonal antibodies directed to different regions of vascular endothelial cadherin extracellular domain affect adhesion and clustering of the protein and modulate endothelial permeability, *Blood*, 2001, **97**, 1679–1684.

47 Y. Chen, L. Ju, M. Rushdi, C. Ge and C. Zhu, Receptor-mediated cell mechanosensing, *Mol. Biol. Cell*, 2017, **28**, 3134–3155.

48 A. S. Yap, K. Duszyc and V. Viasnoff, Mechanosensing and Mechanotransduction at Cell-Cell Junctions, *Cold Spring Harbor Perspect. Biol.*, 2018, **10**, a028761, DOI: 10.1101/cshperspect.a028761.

49 M. A. Garcia, W. J. Nelson and N. Chavez, Cell-Cell Junctions Organize Structural and Signaling Networks, *Cold Spring Harbor Perspect. Biol.*, 2018, **10**, DOI: 10.1101/cshperspect.a029181.

50 C. K. Thodeti, B. Matthews, A. Ravi, A. Mammoto, K. Ghosh, A. L. Bracha and D. E. Ingber, TRPV4 channels mediate cyclic strain-induced endothelial cell reorientation through integrin-to-integrin signaling, *Circ. Res.*, 2009, **104**, 1123–1130.

51 R. Sinha, S. Le Gac, N. Verdonschot, A. van den Berg, B. Koopman and J. Rouwkema, Endothelial cell alignment as a result of anisotropic strain and flow induced shear stress combinations, *Sci. Rep.*, 2016, **6**, 29510.

52 P. C. Dartsch and E. Betz, Response of cultured endothelial cells to mechanical stimulation, *Basic Res. Cardiol.*, 1989, **84**, 268–281.

53 D. E. Conway, B. G. Coon, M. Budatha, P. T. Arsenovic, F. Orsenigo, F. Wessel, J. Zhang, Z. Zhuang, E. Dejana, D. Vestweber and M. A. Schwartz, VE-Cadherin Phosphorylation Regulates Endothelial Fluid Shear Stress Responses through the Polarity Protein LGN, *Curr. Biol.*, 2017, **27**, 2727.

54 N. Baeyens, B. Larrivee, R. Ola, B. Hayward-Piatkowskyi, A. Dubrac, B. Huang, T. D. Ross, B. G. Coon, E. Min, M. Tsarfati, H. Tong, A. Eichmann and M. A. Schwartz, Defective fluid shear stress mechanotransduction mediates hereditary hemorrhagic telangiectasia, *J. Cell Biol.*, 2016, **214**, 807–816.

55 T. Takemasa, K. Sugimoto and K. Yamashita, Amplitude-dependent stress fiber reorientation in early response to cyclic strain, *Exp. Cell Res.*, 1997, **230**, 407–410.

56 S. Jungbauer, H. Gao, J. P. Spatz and R. Kemkemer, Two characteristic regimes in frequency-dependent dynamic reorientation of fibroblasts on cyclically stretched substrates, *Biophys. J.*, 2008, **95**, 3470–3478.

57 U. Faust, N. Hampe, W. Rubner, N. Kirchgessner, S. Safran, B. Hoffmann and R. Merkel, Cyclic stress at mHz frequencies aligns fibroblasts in direction of zero strain, *PLoS One*, 2011, **6**, e28963.

58 K. Nagayama, Y. Kimura, N. Makino and T. Matsumoto, Strain waveform dependence of stress fiber reorientation in cyclically stretched osteoblastic cells: effects of viscoelastic compression of stress fibers, *Am. J. Physiol.: Cell Physiol.*, 2012, **302**, C1469–C1478.

59 R. C. Buck, Reorientation response of cells to repeated stretch and recoil of the substratum, *Exp. Cell Res.*, 1980, **127**, 470–474.

60 A. Livne, E. Bouchbinder and B. Geiger, Cell reorientation under cyclic stretching, *Nat. Commun.*, 2014, **5**, 3938.

61 E. H. Barriga, K. Franze, G. Charras and R. Mayor, Tissue stiffening coordinates morphogenesis by triggering collective cell migration in vivo, *Nature*, 2018, **554**, 523–527.

62 T. E. Angelini, E. Hannezo, X. Trepat, M. Marquez, J. J. Fredberg and D. A. Weitz, Glass-like dynamics of collective cell migration, *Proc. Natl. Acad. Sci. U. S. A.*, 2011, **108**, 4714–4719.

63 A. R. Harris, L. Peter, J. Bellis, B. Baum, A. J. Kabla and G. T. Charras, Characterizing the mechanics of cultured cell monolayers, *Proc. Natl. Acad. Sci. U. S. A.*, 2012, **109**, 16449–16454.

64 D. J. Tschumperlin and S. S. Margulies, Equibiaxial deformation-induced injury of alveolar epithelial cells in vitro, *Am. J. Physiol.*, 1998, **275**, L1173–L1183.

65 D. J. Tschumperlin, J. Oswari and A. S. Margulies, Deformation-induced injury of alveolar epithelial cells. Effect of frequency, duration, and amplitude, *Am. J. Respir. Crit. Care Med.*, 2000, **162**, 357–362.

66 L. Bernardi, R. Hopf, A. Ferrari, A. E. Ehret and E. Mazza, On the large strain deformation behavior of silicone-based elastomers for biomedical applications, *Polym. Test.*, 2017, **58**, 189–198.

67 R. Hopf, L. Bernardi, J. Menze, M. Zundel, E. Mazza and A. E. Ehret, Experimental and theoretical analyses of the age-dependent large-strain behavior of Sylgard 184 (10:1) silicone elastomer, *J. Mech. Behav. Biomed. Mater.*, 2016, **60**, 425–437.

68 J. Schindelin, I. Arganda-Carreras, E. Frise, V. Kaynig, M. Longair, T. Pietzsch, S. Preibisch, C. Rueden, S. Saalfeld, B. Schmid, J. Y. Tinevez, D. J. White, V. Hartenstein, K. Eliceiri, P. Tomancak and A. Cardona, Fiji: an open-source platform for biological-image analysis, *Nat. Methods*, 2012, **9**, 676–682.

69 C. A. Schneider, W. S. Rasband and K. W. Eliceiri, NIH Image to ImageJ: 25 years of image analysis, *Nat. Methods*, 2012, **9**, 671–675.

70 Z. Puspoki, M. Storath, D. Sage and M. Unser, Transforms and Operators for Directional Bioimage Analysis: A Survey, *Adv. Anat., Embryol. Cell Biol.*, 2016, **219**, 69–93.

71 R. Rezakhaniha, A. Agianniotis, J. T. Schrauwen, A. Griffa, D. Sage, C. V. Bouten, F. N. van de Vosse, M. Unser and N. Stergiopulos, Experimental investigation of collagen waviness and orientation in the arterial adventitia using confocal laser scanning microscopy, *Biomech. Model. Mechanobiol.*, 2012, **11**, 461–473.

72 E. Fonck, G. G. Feigl, J. Fasel, D. Sage, M. Unser, D. A. Rufenacht and N. Stergiopulos, Effect of aging on elastin functionality in human cerebral arteries, *Stroke*, 2009, **40**, 2552–2556.

73 M. G. Lampugnani, M. Corada, L. Caveda, F. Breviario, O. Ayalon, B. Geiger and E. Dejana, The molecular organization of endothelial cell to cell junctions: differential association of plakoglobin, beta-catenin, and alpha-catenin with vascular endothelial cadherin (VE-cadherin), *J. Cell Biol.*, 1995, **129**, 203–217.